GEOPHYSICAL RESEARCH LETTERS, VOL. ???, XXXX, DOI:10.1029/,

Assessing possible dynamical effects of condensate in high resolution climate simulations

J. T. Bacmeister, P. H. Lauritzen, A. Dai and J. E. Truesdale

J. T. Bacmeister, Julio Bacmeister, NCAR Earth System Laboratory, National Center for Atmospheric Research, Boulder, CO, 80305. (juliob@ucar.edu)

P. H. Lauritzen, NCAR Earth System Laboratory, National Center for Atmospheric Research, Boulder, CO, 80305

Aiguo Dai, NCAR Earth System Laboratory, National Center for Atmospheric Research, Boulder, CO, 80305

J. E. Truesdale, NCAR Earth System Laboratory, National Center for Atmospheric Research, Boulder, CO, 80305

In areas of heavy precipitation, condensed water species can add significant mass to an atmospheric column. This mass can create positive pressure anomalies of up to several hPa at the surface. This pressure is expected to force a divergent component in the low-level flow that may have an impact on the evolution of the precipitating system. In this study we examine results from a cloud resolving model simulation of tropical convection to estimate the pressure induced by condensates. A simple parameterization of this condensate loading as a function of surface rain rate is derived and implemented in the National Center for Atmospheric Research's Community Atmosphere Model version 5 (CAM5). Our results suggest that at horizontal resolutions of 25 km condensate loading is an important factor in controlling the frequency of intense rain rates in the model.

1. Introduction

The contribution of condensed water species to atmospheric mass has long been known to be a significant factor in the dynamics of moist convection [e.g. Emanuel, 1994; Xu and Randall, 2001]. The weight of condensates in convecting parcels can have a major impact on their buoyancy and may be a dominant control on the global statistics of convection [Emanuel, 1994].

The major contribution to condensate mass comes from precipitating species such as rain, hail, snow, and graupel. Microphysics schemes for models at climate resolutions typically use diagnostic rather than prognostic treatments for precipitating condensate. Climate models correctly account for the removal of mass by precipitation in the models' mass budget. However, the diagnostic treatments in climate models view this removal as occurring instantaneously. In reality precipitating condensate may exist in a deep column that persists for a significant time, i.e., comparable to a typical climate model time step of 15 to 30 minutes. The weight of this column contributes to the pressure field (condensate loading, henceforth abbreviated CL) and can have direct dynamical effects on the flow. The dynamical effects of CL are not currently present in most climate models that use diagnostic treatments of precipitation.

Neglect of CL may be justified at the horizontal resolutions of 100's of km. However, as climate model resolution increases we believe this neglect is no longer justified. This study will assess the potential impact of CL at 25 km resolutions by quantifying the condensate contribution to the pressure field in much finer cloud resolving simulations using the National Center for Atmospheric Research's (NCAR's) Weather Research and

Forecasting model (WRF) [Skamarock and Klemp, 2008]. A simple parameterization of this pressure is developed and implemented in NCAR's Community Atmosphere Model version 5 (CAM5) [Neale et al., 2010]. Our results suggest that horizontal resolutions of 25 km and finer require some representation of CL. This resolution range is already accessible to global climate simulations, and will likely become the default for leading edge simulations in the next ten years. In passing it will be shown that at 25 km and even at 5 km resolutions, CL effects are significantly more important than nonhydrostatic effects.

The paper is structured as follows: In Section 2, we describe the models used in this study. In Section 3 we analyze cloud-resolving model (CRM) results and describe a simple parameterization of CL effects based on surface precipitation rates. In Section 4 we show results from CAM5 including this parameterized CL. In Section 5 we summarize and discuss our results.

2. Models and Experimental Setup

2.1. CAM5

The Community Atmosphere Model version 5 is a state of the art global climate model. Major differences from earlier versions of CAM include a new 2-moment, 2-phase prognostic cloud condensate scheme ,advanced boundary layer and shallow convection schemes and deep convection with enhanced plume entrainment and momentum transport . Complete documentation of CAM5 is provided in [Neale et al., 2010]. In this study we use the finite-volume (FV) dynamical core with a horizontal resolution of $0.23°\text{lat}\times0.31°\text{lon}$ and 30 layers in the vertical. A physics time-step of 15 minutes is used. We will examine results from experiments forced by observed sea-surface temperatures (SST) initialized on Jan 1 2005. The experiments ran for 18 months, but in this study we will examine results from the first 13 months only. Currently CAM5 does not incorporate any condensed water species in its atmospheric mass field.

2.2. WRF

The Weather Research and Forecasting model is a well established nonhydrostatic dynamical model with flexible nesting capability [Skamarock and Klemp, 2008]. WRF solves the full Euler equations on a dry mass vertical coordinate. Prognostic equations for pressure, 3D velocity, heat, and water species are included. In this study we will examine results from the innermost domain of triply-nested simulation initialized by ERA interim reanalysis. The simulation period covers February 22 through 27 2005. The innermost domain has a resolution of 500 m in both zonal and meridional directions with a size of 1000×800 gridpoints. It is chosen to overlap with the TOGA-COARE domain; 112°E to 117°E and 5°S to 1°S. Fifty vertical levels are used with a top close to 25 km, and Δz ranging from 50 m close the surface to 500 m in the midtroposphere. A 2 second time step is used and data are saved every 15 minutes.

WRF offers a large number of options for parameterizing physical processes, including cloud microphysics. The experiment examined here used the Hong and Lim [2006] microphysics option. This is a 6-category bulk scheme that incorporates graupel rather than hail, as appropriate for tropical, oceanic convection. The innermost domain in the simulation discussed here did not employ a deep convection parameterization.

3. Development of condensate loading (CL) parameterization

3.1. Preliminary analysis of WRF results

WRF uses a complete prognostic pressure equation, which includes nonhydrostatic effects as well as a complete atmospheric mass field, including the contribution of all condensed water species. Our assessment of the potential CL effect at high climate resolutions (25 km) involves two steps. First, the CRM fields are coarse grained to 25 km resolution by averaging over 50×50 gridpoint subdomains. Second, coarse-grained profiles of potential temperature $\overline{\theta}$ (K), water vapor mixing ratio with respect to dry air $\overline{q}_w$ (kg kg^{-1}), and condensed water mass mixing ratios with respect to dry air $\overline{q}_{[l,i,r,s,g]}$ (kg kg^{-1}), where the subscripts l, i, r, s, and g refer to cloud liquid, cloud ice, rain, snow, and graupel, are used to calculate diagnostic hydrostatic pressure fields with and without CL

$$\overline{\pi}_{hyd,[v,c]}(x,y,z,t) = \overline{\pi}_{top} + \int_{z}^{z_{top}} \frac{g}{c_p \overline{\theta}_{[v,c]}(x,y,z',t)} dz', \tag{1}$$

where g is gravitational constant (9.81 m s^{-2}), c_p is specific heat capacity of dry air (1003 J kg^{-1}). The Exner pressure π_{hyd} and the pressure are related by

$$\overline{p}_{hyd} = p_{00} \left(\overline{\pi}_{hyd}\right)^{c_p/R}, \tag{2}$$

where R is gas constant for dry air (286 J kg^{-1}), and p_{00} is a reference pressure of 1000 hPa. We use two versions of thermodynamic variable $\overline{\theta}_{[v,c]}$ in the hydrostatic integral (1)

$$\overline{\theta}_v = \overline{\theta} \frac{1+\overline{q}_w/\epsilon}{1+\overline{q}_w} \tag{3}$$

$$\overline{\theta}_c = \overline{\theta} \frac{1+\overline{q}_w/\epsilon}{1+\overline{q}_w+\overline{q}_l+\overline{q}_i+\overline{q}_r+\overline{q}_s+\overline{q}_g} \tag{4}$$

[e.g. Emanuel, 1994, (4.3.6)]. With $\overline{\theta}_v$ the diagnostic hydrostatic pressure $\overline{p}_{hyd,v}$ obtained from (1) will include virtual effects but not CL. This quantity is the pressure variable used in most state-of-the-art climate models. Using $\overline{\theta}_c$ in (1) yields an approximate hydrostatic pressure including both virtual effects and CL.

Figure 1 shows joint frequency distributions (JFDs) of $\overline{p}_{hyd,c}$ and $\overline{p}_{hyd,v}$ at the surface versus the coarse grained prognostic pressure from WRF $\overline{p}$. Fig. 1b shows that ignoring CL even at 25 km resolutions leads to frequent, large surface pressure departures from the WRF value. Underestimates of several hPa are common. A clear implication of this result is that high-resolution climate model surface pressures in regions of strong precipitation may be systematically underestimated by several hPa. In the tropics, pressure anomalies of this size may be dynamically-significant. The CL effect on pressure should act against low-level convergence, and should therefore weaken CISK(Conditional Instability of the Second Kind)-interactions between moist heating and flow in the boundary layer.

The close agreement between $\overline{p}_{hyd,c}$ and $\overline{p}$ in Fig. 1a implies that nonhydrostatic dynamics are unimportant at the 25 km scale. So, while small, intense, nonhydrostatic updrafts may be critical in determining vertical fluxes, their detailed structure has negligible impact on the pressure field at scales of 25 km. Based on this analysis there is no reason to suspect that explicitly-resolved convection in a model with 25 km resolution would be inherently "pathological". We repeated this analysis using a coarse-graining scale of 5 km (10×10 WRF points). Results are summarized in Table 1. As expected, the root mean square (RMS) difference between $\overline{p}_{hyd,c}$ and $\overline{p}$ is larger than for the 25 km scale. Nevertheless, even at 5 km the difference between $\overline{p}_{hyd,v}$ and $\overline{p}$ is still much larger than that between $\overline{p}_{hyd,c}$ and $\overline{p}$, suggesting that CL remains more critical at 5 km resolution than nonhydrostatic dynamics.

3.2. Implementation of CL parameterization in CAM5

In order to quickly assess potential CL impacts, we designed a simple parameterization for CAM5 based on surface precipitation rates. Figure 2 shows a JFD of CL-induced surface pressure, i.e., $p'_{CL} \equiv \overline{p}_{hyd,c} - \overline{p}_{hyd,v}$ at z=0, and 15-minute average, surface rain rate $\mathcal{R}_{sfc}$ from our WRF simulation. The plot shows that a reasonably-compact, relationship exists between these variables. The additional hydrostatic pressure induced by CL at any height z is given by

$$p'_{CL}(x,y,z,t) = \int_z^\infty g\rho_c(x,y,z',t) \quad dz' \tag{5}$$

where ρ_c is the density of all condensate in the atmosphere. Examination of condensate density profiles from our WRF simulations binned by $\mathcal{R}_{sfc}$ (supplemental Figure 1) suggests ρ_c is reasonably constant from the surface to around 5000 m and then begins to drop off rapidly somewhere between 5000 and 10000 m. This general shape seems to hold for moderate to intense $\mathcal{R}_{sfc}$ (100 to 1000 mm d^{-1}).

As a crude first approximation we set ρ_c to a constant value ρ_{c0} between the surface and a height H_{CL} and set ρ_c=0 above. The density ρ_{c0} is then specified as a function of $\mathcal{R}_{sfc}$ and a terminal velocity w_f,

$$\rho_{c0} = \rho_{L0} \frac{\mathcal{R}_{sfc}}{w_f}. \tag{6}$$

where ρ_{L0} is the density of liquid water (1000 kg m^{-3}) and $\mathcal{R}_{sfc}$ is expressed in units of m s^{-1}. Combining (5) and (6) and incorporating our assumptions about the shape of the condensate profile we obtain an expression for the time-varying, fully-3D, hydrostatic pressure perturbation induced by CL

$$p'_{CL}(x,y,z,t) = \begin{cases} g\rho_{L0}\frac{\mathcal{R}_{sfc}}{w_f} \times (H_{CL} - z) & z \leq H_{CL}, \\ 0 & z > H_{CL}. \end{cases} \tag{7}$$

For $\mathcal{R}_{sfc}$ we use the instantaneous CAM5 total surface precipitation (convective+large-scale) at each time step. We simply use the hydrostatically-determined heights of the CAM5 half-levels or layer edges to define the condensate column. When the upper-edge of a layer falls below H_{CL} it is included in the column, otherwise it is left out. This can lead to some variation in the actual thickness of the condensate layers.

The condensate pressure p'_{CL} is added to the dynamical pressure in the FV dynamical core immediately before horizontal pressure gradient forces are calculated. In the present implementation p'_{CL} has no other effects in the simulation, so that its horizontal gradient can simply be regarded as another parameterized body force similar to gravity wave drag.

We tried 2 different forms for p'_{CL} (Table 2) whose surface signatures are shown by the white lines in Fig. 2. These two experiments are intended to explore the sensitivity of the model to the depth of CL while maintaining the CL pressure signature at the surface approximately constant. Clearly, CL1 with H_{CL}≈8500m is closer to the WRF condensate profiles (supplemental Fig. 1) than is CL2 with H_{CL}≈2000m. However, it should be kept in mind that these profiles are from a single 5-day period dominated by deep convection. Furthermore, as will be seen below CL2 reveals interesting sensitivities to H_{CL}.

4. CAM5 results

Figure 3a shows probability density functions (PDFs) of instantaneous precipitation intensity (30°S-30°N) in our CAM5 experiments, accumulated during August 2005 from data written every 3 hours. The PDF from the CAM5 control (CTR) is shown in black.

The observational PDF for precipitation estimated from the Tropical Rainfall Measuring Mission (TRMM) 3B42 product [Huffman et al., 2007] is also shown (dashed red). CTR clearly overestimates the likelihood of precipitation rates greater than 200 mm d^{-1} with respect to TRMM-3B42. There is some uncertainty about whether the TRMM-3B42 precipitation rates represent instantaneous values or longer three hour averages. In any case, there is minor impact on the model PDFs in Figure 3a when three hour average precipitation rates are used (see supplemental Figure 2). Boyle and Klein [2010] note that excessive extreme precipitation becomes more pronounced in CAM as resolution increases. We also note that observations of intense precipitation frequency are likely to depend on the area sampled, with smaller sample area yielding more frequent intense events.

With parameterized pressure gradient forces from CL, the frequency of intense precipitation rates ($\mathcal{R}_{sfc}$>200 mm d^{-1}) is dramatically reduced. In CL1 only a small excess with respect to TRMM at these rates remains (Fig. 3a, green curve). The result for CL2 (magenta curve) is similar to CL1 for $\mathcal{R}_{sfc}$ <1000 mm d^{-1}, but at higher rates CL2 is less effective at reducing occurrence probabilities. This suggests that a deep pressure perturbation is better at suppressing these wildly extreme events. In all cases, the effect of CL is remarkably well targeted at reducing the frequency of intense precipitation. At rates below 100 mm d^{-1} little effect from CL is noticeable.

Figure 3b shows PDFs of vertical motion near 850 hPa (ω_{850}) over tropical ocean. There is a clear connection between large precipitation rates and integrated low-level convergence, indicated by ω_{850}<0. The control simulation exhibits a pronounced skew towards strong convergence events. This skew is significantly reduced in CL1. In CL2 moderate convergence (-4000 to -2000 hPa d^{-1}) is noticeably more suppressed than in CL1, but strong convergence (<-6000 hPa d^{-1}) is almost as frequent as in CTR again suggesting a connection between large H_{CL} and suppression of extremes.

Figure 4 shows 12-month mean precipitation from CAM5 compared with observational estimates from the Global Precipitation Climatology Project [GPCP, Adler et al., 2003]. All CAM5 experiments exhibit positive precipitation biases in the Pacific intertropical convergence zone (ITCZ) with respect to GPCP. Modest improvements over CTR (Fig. 4a) are evident in CL1 (Fig. 4b) particularly south of the Equator where the model's double ITCZ bias has been reduced. Interestingly, in CL2 (Fig 4c) clearer improvements in mean precipitation are seen, with peak values dropping by around 3 mm d^{-1} over much of the northern ITCZ. This suggests that the suppression of moderate low-level convergence seen in Fig. 3b may be more significant in determining some aspects of mean model climate than the suppression of extremes.

5. Summary and Discussion

We have shown that a simple but plausible parameterization of condensate loading (CL) has appreciable impacts on simulations with the Community Atmosphere Model version 5 (CAM5) at a horizontal resolution of 0.23°lat×0.31°lon. Our parameterization assumes a one-to-one relationship between instantaneous surface precipitation rates and the total mass of condensates in the atmospheric column above. The condensates are assumed to have constant density in a layer of specified thickness H_{CL} and to fall with terminal velocity w_f. Three CAM5 experiments with CL were performed using values of w_f and H_{CL} given in Table 2. The surface signatures of the resulting condensate pressure are compared with those from a 5-day cloud resolving simulation of tropical convection using the Weather Research and Forecasting model (WRF) in Figure 2.

The best overall fit to the WRF results (CL1) yields significant reductions in the frequency of intense precipitation ($\mathcal{R}_{sfc}$>200 mm d^{-1}) and intense low-level convergence (ω_{850}<-6000 hPa d^{-1}) (Fig. 3), as well as modest improvements in annual mean precipitation patterns (Fig. 4). Reducing the assumed thickness of the condensate layer (CL2), while maintaining the surface pressure signature close to that in CL1, reduces the impact of CL on the frequency of intense precipitation and convergence. On the other hand, moderate convergence events (Fig. 3b) and annual mean precipitation in the ITCZ (Fig. 4c) are more strongly suppressed in CL2. This suggests that letting H_{CL} increase with $\mathcal{R}_{sfc}$ could yield improvements in both climate means and extreme event statistics.

We note that our parameter choices in designing the CL parameterization are based on a single 5-day WRF experiment. Both the meteorological background state and the choice of microphysics scheme for the WRF experiment could affect the estimate of CL as a function of surface precipitation rate as well the vertical profile shape chosen to represent the condensates. However, there is no reason to believe that the WRF results used here grossly misrepresent these quantities, and for an exploratory study such as this, we believe this is sufficient.

Acknowledgments. NCAR is supported by the National Science Foundation. This work was was also supported by a grant from the Department of Energy's Office of Biological and Environmental Research.

References

Adler, R., et al., 2003: The Version 2 Global Precipitation Climatology Project (GPCP) Monthly Precipitation Analysis (1979- Present). *Journal of Hydrometeorology*, **4 (1)**, 1147–1167.

Boyle, J. and S. Klein, 2010: Impact of horizontal resolution on climate model forecasts of tropical precipitation and diabatic heating for the TWP-ICE period. *Journal of Geophysical Research*, **115 (D23)**, D23 113.

Emanuel, K., 1994: *Atmospheric Convection*. Oxford University Press, USA.

Hong, S. and J. Lim, 2006: The WRF single-moment 6-class microphysics scheme (WSM6). *J. Korean Meteor. Soc*, **42 (2)**, 129–151.

Huffman, G., et al., 2007: The TRMM Multisatellite Precipitation Analysis (TMPA): Quasi-global, multiyear, combined-sensor precipitation estimates at fine scales. *Journal of Hydrometeorology*, **8 (1)**, 38–55.

Neale, R., C.-C. Chen, A. Gettelman, P. Lauritzen, S. Park, D. Williamson, and et al., 2010: Description of the NCAR Community Atmosphere Model (CAM 5.0). *NCAR Technical Note*, **NCAR TN (486)**.

Skamarock, W. and J. Klemp, 2008: A time-split nonhydrostatic atmospheric model for weather research and forecasting applications. *Journal of Computational Physics*, **227 (7)**, 3465–3485.

Xu, K. and D. Randall, 2001: Updraft and downdraft statistics of simulated tropical and midlatitude cumulus convection. *Journal of the Atmospheric Sciences*, **58 (13)**, 1630–1649.

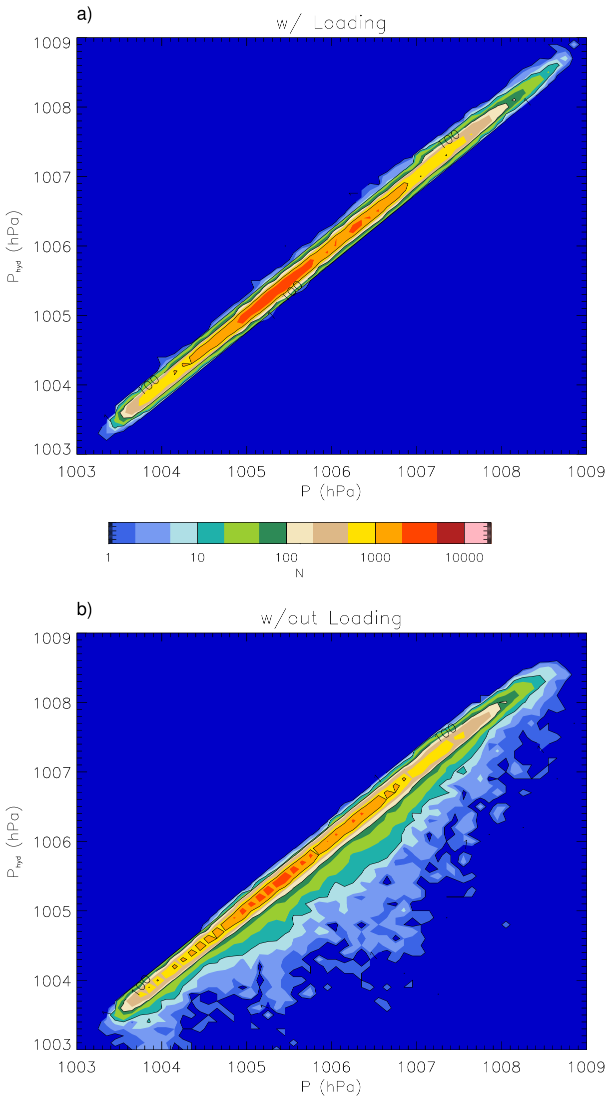

Figure 1. JFDs of prognostic WRF pressure (horizontal) vs. diagnostic hydrostatic pressure calculations (vertical). Hydrostatic pressures are calculated using fields coarse-grained to 25km×25km subdomains. Panel a shows result with a hydrostatic calculation including mass of all condensed species. Panel b shows result for hydrostatic calculation ignoring condensate masses (see text). N is the number of occurrences in each 0.1×0.1 (hPa^2) bin

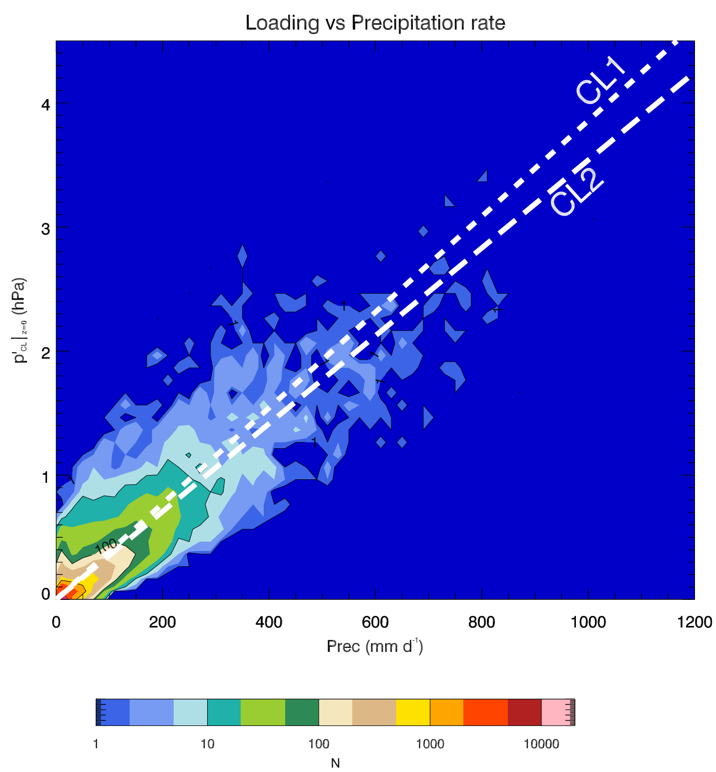

Figure 2. JFD of pressure loading at the surface from condensates (hPa, vertical axis) and surface precipitation rates $\mathcal{R}_{sfc}$ (mm d^{-1}, horizontal axis) in 25km×25km subdomains. Dashed White lines show $p'_{CL}|_{z=0}$ for CL1 and CL2 defined in Table 2. N is the number of occurrences in each 20×0.1 (mm d^{-1}×hPa) bin.

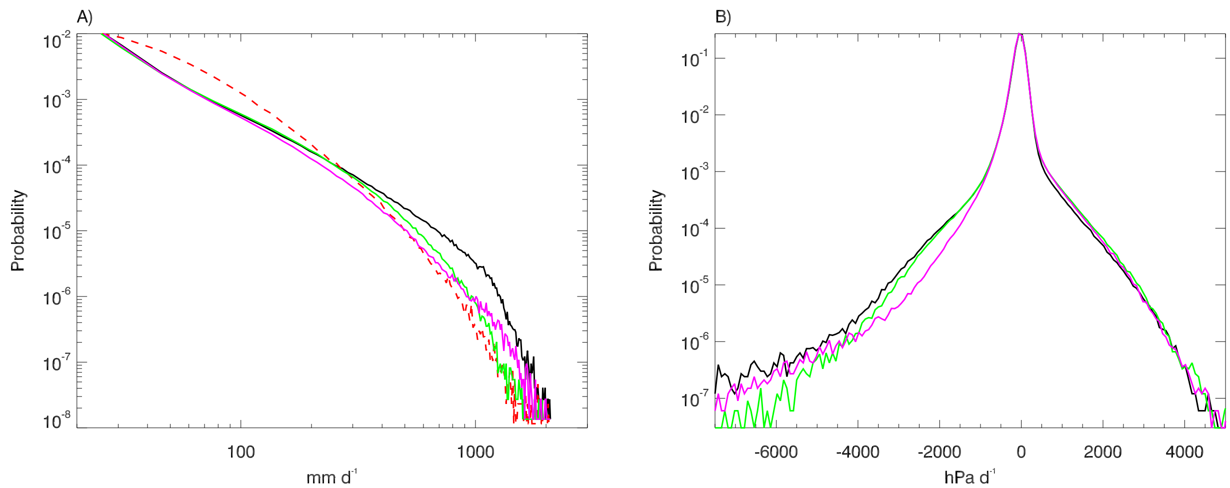

Figure 3. a) PDFs of precipitation rates for August 2005 between 30°S and 30°N for experiments defined in Table 2: CTR (black curve); CL1 (green curve); and CL2 (magenta curve). The corresponding TRMM 3B42 observational estimate is shown by the dashed red curve. Note results are displayed in log-log form. b) Same as except for vertical motion around 850 hPa (ω_{850}) over ocean, between 12°S and 25°S. Note only vertical axis is logarithmic in panel b. Probabilities are with respect to bins of 15 mm d^{-1} (a) and 80 hPa d^{-}1(b).

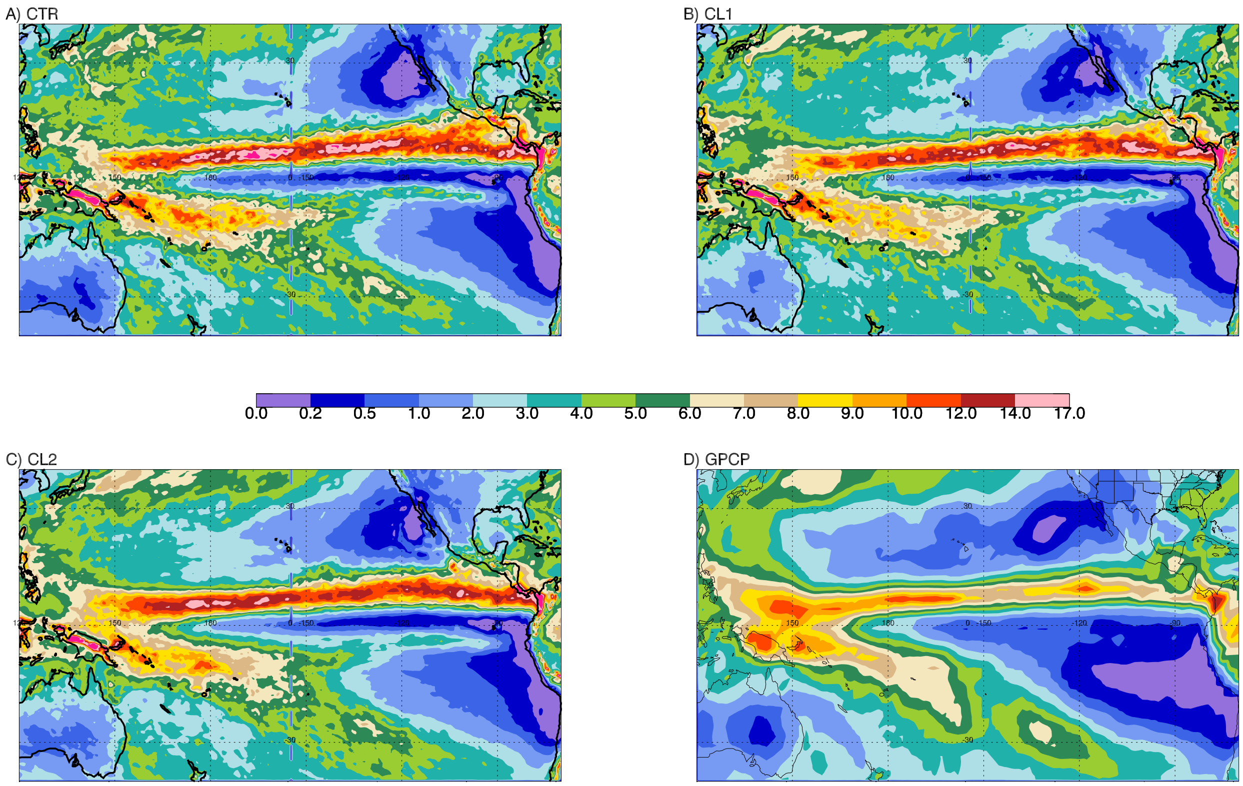

Figure 4. 12-month mean surface precipitation rate for 2/2005-1/2006 as a function of longitude and latitude for: a) CTR; b) CL1; c) CL2; and d) from the GPCP observational estimate.

Table 1. RMS differences between p_{wrf} and p_{hyd} for different coarse-graining scales

Coarse-graining scale	w/ loading (hPa)	w/out loading (hPa)
25 km	0.062	0.17
5 km	0.098	0.25

Table 2. CAM5 experiments and parameters for p'_{CL}

Experiment	w_f	H_{CL}
CTR	control, no loading	
CL1	2.5 ms^{-1}	8500 m
CL2	0.625 ms^{-1}	2000 m